DYNAMIC STALL ON A SUPERCRITICAL AIRFOIL

W.Geissler*), G.Dietz**), H.Mai**)
German Aerospace Centre (DLR), Göttingen

Abstract:
For the present investigations of dynamic stall a supercritical airfoil was chosen. This new airfoil designed by DLR will be used in dynamic stall control research activities (project ADASYS) planned for the near future: The leading edge portion of the airfoil will be drooped down dynamically to improve dynamic stall characteristics on the retreating side during blade motion. The optimised transonic properties of the airfoil, i.e., reduction of shock strength over a Mach number range will improve in addition the performance of the advancing rotor blade.
Dynamic stall experiments on the rigid supercritical airfoil have first been carried out in the DNW-TWG transonic wind tunnel with a 1mx1m cross section of the test section and adaptive top and bottom - walls. This tunnel has the advantage to cover the speed range of both retreating and advancing blade. Emphasis has been placed on unsteady pressure measurements along the adaptive walls simultaneously with the unsteady pressure measurements on the pitching model.
In addition to the experiments corresponding numerical simulations with a RANS-code have been carried out and their results are compared with the experimental data.
Of main concern are the influence of laminar-turbulent boundary-layer transition as well as wind-tunnel-wall interference effects on the unsteady results.

1. Introduction

The present experimental and numerical study is intended to be a preparation phase for the more comprehensive test utilizing a dynamic nose-droop device at the leading edge of the blade model. For these investigations a supercritical airfoil has been developed by DLR using the design software of [1]. This airfoil has been demonstrated to have very good properties in the transonic flow regime but of course is not very suitable under dynamic stall conditions. The main objective of the running project ADASYS (DLR/ECD/EADS-cooperation) will be the improvement of the dynamic stall properties with the application of a 10%-leading edge portion of the airfoil drooping down by a maximum deflection angle of $\delta=10^o$. This motion will be realized by a system of piezo-electric actuators inside the model moving the leading edge downwards from the datum airfoil to the maximum deflection angle and back. In addition to the blade deflection the model is oscillating about its quarter chord axis simulating the cyclic pitch motion of the blade in forward flight.
The complicated test set-up for these wind tunnel investigations has already been used in a similar way during the RACT-project (Rotor Active Control Technology, [2]): In this case the 15%-trailing edge flap oscillated with a frequency up to 5/ref of the cyclic motion (7Hz) of the blade model. The actuators used in the RACT-tests are the same, [3] as in the planned drooping tests.
Several numerical investigations have already been done to study the effects of drooping airfoils on dynamic stall properties. A typical helicopter airfoil has been used in [4] adding a nose-droop device to control dynamic stall. It has been shown that the drag rise as well as the impulsive negative pitching moment could be reduced considerably without loosing too much lift.
Recently experiments have been documented [5] for a blade model with a 25% leading edge droop device. In this special case the drooping angle corresponded to the angle of incidence during the oscillatory motion of the model.
Both calculation and experiment have shown considerable benefit of the drooping device.
The present study uses a completely new transonic airfoil design called A1510-airfoil in the DLR nomenclature. The design method of this supercritical airfoil has already been described in [6].
The objective of the present first step of the ADASYS project is to study the behaviour of the supercritical rigid airfoil under dynamic stall conditions.
The wind tunnel facility used for the test, i.e., the DNW-TWG has the property to cover the low speed (M>0.3) as well as the transonic speed

*) Senior Research Scientist, Institute of Aerodynamic and Flow Technology
**) Research Scientist, Institute of Aeroelasticity

regime. The properties of the blade model can be studied for advancing and retreating blade velocities without changing the model or the test set-up. Furthermore, the adaptive test section of the wind tunnel has been used for the first time in dynamic stall measurements. New insight into the role of wind-tunnel-wall interference effects on the unsteady air loads are to be expected.
Numerical calculations have been added for comparison using a 2D-time-accurate RANS-code [7]. This code has been proven to gain reliable results for dynamic stall flow cases although the influence of turbulence and laminar-turbulent boundary-layer transition modelling may be a limiting factor with respect to the reliability of the numerical results. The application of transition modelling will be given specific concern in the present calculations.

2. Motivation

The use of a supercritical airfoil design for dynamic stall investigations has to be assumed as part of a more comprehensive project, i.e., the ADASYS project with the objective to control dynamic stall by means of a nose-drooping device.
Fig.1 shows the shape variation of the drooping airfoil ready for implementation into the numerical code.

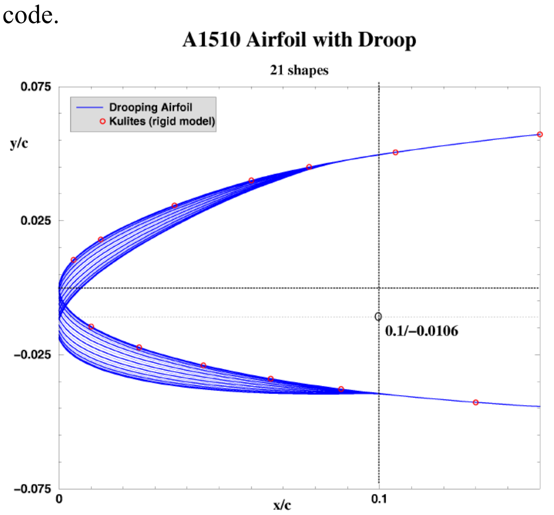

Fig.1: Shape Variation of A1510 Airfoil

The nose-drooping concept has been investigated mainly numerically but recently also experimentally [5] to show impressive benefits with respect to dynamic stall characteristics: Drag and pitching moment peaks could be reduced considerably keeping the maximum lift at a high level.
The ADASYS project follows a new idea: Design the airfoil for the transonic flow regime, i.e., for Mach numbers extending M=0.7 in an optimised way and then add a drooping device for the retreating sector of the blade cycle to alleviate dynamic stall. The advantage of this concept is obvious: Keeping the droop angle at zero for the advancing side of the motion to gain the benefit of reduced shock strength of the transonic airfoil and adding droop dynamically for the retreating side to improve dynamic stall properties.
Although the realisation of the drooping device is a challenging task, it is avoided to apply additional devices for the advancing blade.
In the present investigations the properties of the designed airfoil shape A1510 under transonic flow conditions will be studied and compared with numerical data. The behaviour of the supercritical airfoil under dynamic stall conditions will be studied for different Mach numbers, frequencies and incidence variations. From these first unsteady tests the amount of benefit with versus without nose-drooping will be shown in future tests.

3. Wind tunnel

The present experiments have been carried out in the DNW-TWG transonic wind tunnel located at DLR-Göttingen, Germany. The Mach number can be reduced to M=0.31 as the lowest and cover therefore most of the helicopter relevant Mach range including the transonic flow regime relevant for the advancing part of the cycle.
The TWG is a continuously working wind-tunnel with a 1mx1m squared adaptive test section equipped with pressure sensors along the walls to measure instantaneous static pressures. The ratio of the tunnel height to the chord of the investigated airfoil model is 3.33. Therefore the top and bottom walls of the test section were adapted to the flow. The steady wall interference is minimized by a one step method of wall adaptation based on a Cauchy type integral [8] using the time averaged pressure data and the actual wall position. The displacement thickness of the turbulent wind-tunnel wall boundary layer is predicted by Head's method [9] and is added to the wall shapes; top and bottom wall displacement thicknesses are obtained according to the measured pressure gradients at each wall while the gradient is neglected for the sidewalls [10]. The residual wall interference will be discussed in Section 6.3.

4. Test Set-up

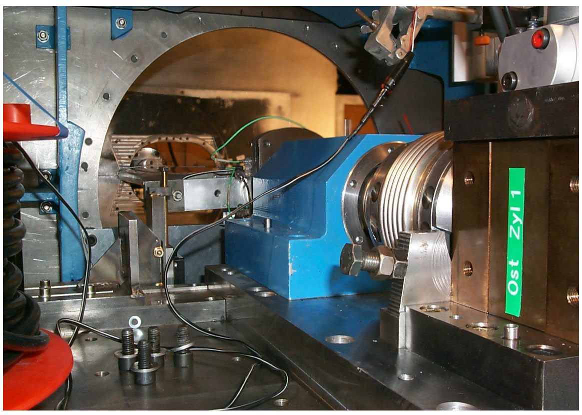

Fig.2: Test Set-up in the Adaptive Wall Test Section of the DNW-TWG

The test set-up provides an actuation system that forces pitch oscillations of the airfoil by means of hydraulic rotation cylinders. The airfoil is mounted on each side to a piezoelectric balance of high stiffness [11] in order to measure the steady airloads lift, drag and pitching moment as well as the unsteady root loads. Two laser triangulators on each side of the test section measure the instantaneous heave and pitch of the model. **Fig.2** shows the model in the test section of the tunnel including the hydraulic driving mechanism.

The airfoil model was shaped as the supercritical A1510 airfoil with the contour developed in [6]. The model is made of a carbon-fiber composite structure having a chord of 0.3 m and a span of 1 m. It is light weight, very stiff and may be assumed to be rigid. In order to investigate the flow around the forced oscillating airfoil, the model is equipped with 46 miniature pressure transducers Kulite XCQ-093-5psi measuring both steady and unsteady pressure differences with reference to the wind tunnel's plenum pressure. Furthermore, one accelerometer PCB 352C22 is located in the rear part of the model. These sensors are arranged beneath the model surface and the pressure taps of 0.3 mm diameter are located in the middle chord at 50% span. The surface of the model is wet grinded with a 1200 grain and is expected to have a peak-to-valley surface roughness lower than 20 µm.

The DLR AMIS II system based on the device TEDAS was applied for data acquisition and processing. The AMIS II provides up to 360 data channels with a maximum sampling frequency of 40 kHz per channel using delta sigma technology.

Standard feature is the online and offline processing of the test data. The data acquisition has been synchronised with the pitching motion of the model such that 128 samples were recorded per cycle.

5. Numerical investigation

In addition to measurements numerical calculations have been done with a software system developed at DLR, [7]. This software has been specifically developed for unsteady separated flows like dynamic stall on oscillating airfoils or buffet on fixed airfoils. The software system has different components including grid generation (structured grids), design procedure for transonic airfoils and steady as well as unsteady numerical solution procedures based on the full Navier-Stokes equations.

Of special concern is the application of turbulence and transition modelling. In the present investigations two different turbulence models have been applied and tested in comparison with the experimental data. Special emphasis is placed on the development and application of transition models suitable for unsteady and separated flows.

5.1 Code

The numerical integration is based on the approximate factorisation implicit procedure developed originally by Beam and Warming, [12]. The finite difference method uses central differencing taking into account artificial viscosity, [13]. A special feature of the code is the ability to deform the grid with respect to time: This option is important in cases of dynamically deforming airfoils, i.e., for oscillating trailing or leading edge flaps (see Fig.1).

5.2 Transition and Turbulence Modeling

Recent numerical calculations with the present software system have shown that the application of the Spalart-Almaras (SA) turbulence model, [14] gives the most reasonable results compared to experimental data, [15]. This holds definitely for unsteady separated flow problems like dynamic stall. However, at higher Mach numbers, i.e., for transonic flows the more sophisticated k-omega SST model of Menter, [16] shows improvements. The sensitivity of the models with respect to separation onset is different for both models: The SA model shows less sensitivity, separation onset is shifted slightly to higher incidences. The k-omega model gives better results for steady flows. However, in cases of airfoil oscillations the model shows too high sensitivity in separated flow areas and tends to unphysical oscillations. Keeping these experiences in mind the following dynamic stall calculations have been carried out only with the SA-model.

In recent years dynamic stall calculations mostly were done with the simplified assumption of fully turbulent boundary-layer flow. This assumption however is not adequate as has been demonstrated experimentally in [17].

During the up-stroke motion of the airfoil a laminar separation bubble may develop with turbulent reattachment of the flow at the end of the bubble. At higher incidences this bubble may burst or collapse and initiate dynamic stall onset.

The successful modelling of these very complicated flow effects is a formidable task. Nevertheless first steps towards realisation of a suitable transition model for dynamic stall application have been done and this model has first been tested in [18]. The model works in a quasi-steady manner, i.e., for each time-step the transition from laminar to turbulent flow is calculated separately assuming quasi- steady flow state.

Of strong concern is the determination of transition onset: The present wind tunnel measurements have all been done without transition strip allowing free transition. This makes it necessary also in the calculation to predict the instantaneous position of transition onset. This difficult task has been achieved by the application of Michel's criterion, [18]. Unfortunately, a direct comparison of the predicted transition region and experimental results is not possible, since measuring the transition

region in unsteady flow would exceed the scope of the test campaign and was not performed.
However, in the following discussions of results the effect of transition on dynamic stall characteristics will be investigated in some detail.

Dynamic Stall Experiments in TWG (September 2002)
Test Matrix

Table 1:

Nr	Ma	α_0 [deg]	α_1 [deg]	$\omega^* = 2*\pi*f*c/U_\infty$	Remarks
1	0.31				Steady Polar
2	0.35				Steady Polar
3	0.40				Steady Polar
4	0.31	15	5/10	0.05/0.1/(0.2)	Unsteady with WT-Wall Adaption at α_0/α_{sep}
5	0.31	10	5/10	0.05/0.1/(0.15)/(0.2)	" ω^* values in Brackets for small α_1 only
6	0.31	5	5	0.05/0.1/0.15/0.2	"
7	0.35	15	10	0.05/0.1	"
8	0.35	10	10	0.05/0.1	"
9	0.40	15	5	0.05/0.1/0.2	"
10	0.40	10	5/10	0.05/0.1/(0.15)/(0.2)	"
11	0.40	5	5	0.05/0.1/0.15	"
12	0.71				Steady Polar
13	0.73				Steady Polar
14	0.75				Steady Polar

α_1 is nominal (actual values partly reduced at higher frequencies)

DLR

W.Geissler, DLR-AS, January 2003

Table 1: Test Matrix

6. Results

Table 1 includes the test matrix of the DNW-TWG dynamic stall measurements in September 2002. In addition to cases with oscillating model, steady polars have been measured both in the low speed as well as in the transonic flow regime. The steady transonic data are of importance to study the performance of the supercritical A1510 airfoil under design conditions, i.e., at M=0.73 and α=2^o incidence.
The unsteady cases have been measured at three Mach numbers: M=0.31/0.35/0.40. In the higher Mach number cases considerable compressibility effects on the dynamic stall characteristics are to be expected. In most of the unsteady cases the reduced frequency ω^* (referred to chord, see Table 1) has been varied between 0.05 and 0.2. To cover also cases without severe separation the mean incidence α_o as well as the amplitude α_1 have been limited to 5^o and 10^o. Mild dynamic stall is to be expected at α_o=10^o and α_1=5^o. Main emphasis has been placed on deep dynamic stall cases with α_0=10^o/15^o and α_1=10^o.
During the tests wind tunnel wall adaptation has been applied. For the steady polars the standard wall adaptation procedure (cf. Section 3) has been performed for each incidence of the different polars separately. In the unsteady cases a wind tunnel adaptation procedure is not straightforward. In the present tests a steady wind tunnel wall adaptation has been applied for **one incidence** of the oscillation cycle only. This incidence has been the mean incidence of the cycle: α_o. In addition a second adaptation has been done at an incidence somewhat larger (smaller) i.e. close to the angle of attack at which separation has been measured for the steady polars. The wind tunnel wall shape for these incidences has been kept for the entire oscillation loops. Due to wind tunnel wall adaptation with two different incidences the number of test cases shown in Table 1 is doubled.

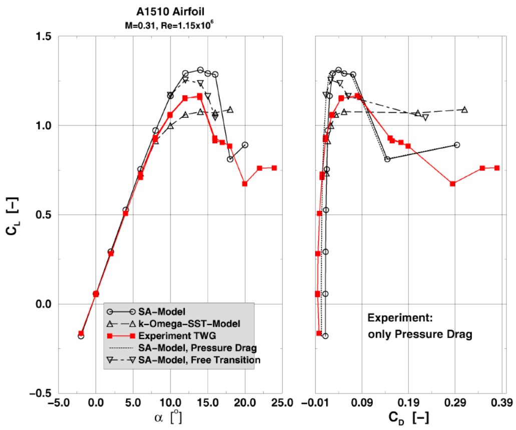

Fig.3: Steady Polar at M=0.31

6.1 Steady data

Fig.3 shows the lift- and drag polars for the low Mach number M=0.31. In addition to the experimental data three different numerical results are displayed: 1) calculation with the SA turbulence model, fully turbulent, 2) with the SA-Model, free transition 3) with the k-omega-SST model, fully turbulent. Due to the fact that the measured drag has been determined from integration of surface pressures, only the pressure drag can be displayed. Calculated pressure drag has been included in the drag polar as well. In the lower incidence regime up to α=10^o the correspondence between calculation and experiment is very good. This is also the case for the pressure drag in this regime. In the higher incidence regime remarkable differences occur between calculation and experiment but also between the different calculations. The SA-model shows less sensitivity with respect to separation and reaches therefore to higher C_{Lmax} values. The k-omega model however seems to be too sensitive and separation for this model occurs too early. The experimental data are in between these calculations. A further improvement is achieved with the implementation of the transition modelling combined with the SA model. C_{Lmax} as well as the behaviour

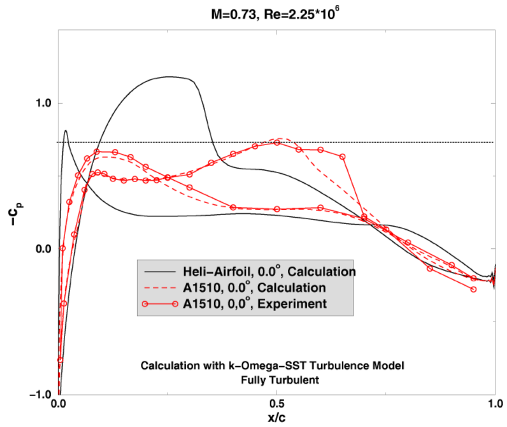

Fig.4a: Steady Pressures at Transonic Speed Typical Helicopter Airfoil Versus A1510, α=0°

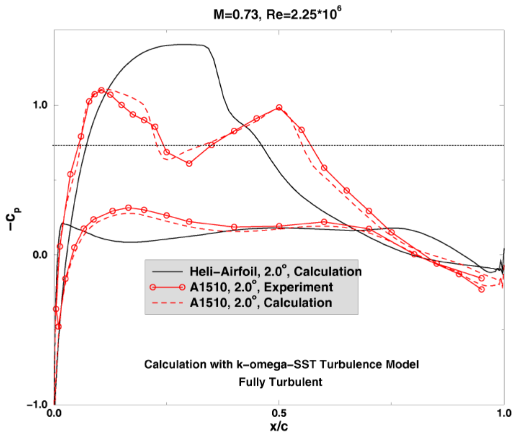

Fig.4b: α=2°

in the separated flow regime is considerably improved compared to the test data.

Figs. 4a and 4b show steady pressure distributions for the transonic Mach number M=0.73 which is the design Mach number for the supercritical airfoil A1510. Fig.4a includes the calculated and measured pressures for α=0°, Fig. 4b displays the results for α=2°. The latter case is the design condition for the A1510 airfoil. In addition to the pressure distributions for the A1510 airfoil the corresponding calculated pressure distributions for a typical modern helicopter airfoil has been included. Even at α=0° this airfoil shows a large supersonic area terminated by a strong shock wave which is increasing in strength for the higher incidence case (Fig.4b). The supercritical airfoil shows almost subsonic flow in the zero incidence case. At α=2° (Fig.4b) the supercritical airfoil shows only minor supersonic areas with a mild shock wave. The correspondence between calculation and experiment is satisfactory. It has been found recently that the k-omega-SST turbulence model has advantages at transonic Mach numbers. This is represented by a better matching of the shock location compared with experiments as well as the correct prediction of buffet onset. The k-omega model has been used for the present steady transonic calculations displayed in Figs.4.

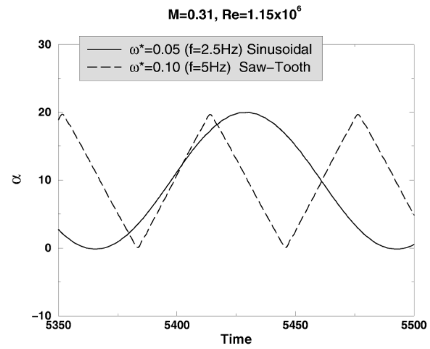

Fig.5: Sin-Wave and Saw-Tooth Incidence Variation

6.2 Unsteady data

For the discussion of the unsteady results deep dynamic stall cases have been selected in the present paper. In these cases the amplitude of oscillations is about α_1=10°. Unfortunately, the hydraulic actuators are limited in both the maximum torque moment and thus in the achievable acceleration as well as in the flow rate and thus in the maximum angular velocity. Therefore, the available actuators have limitations for simulating helicopter relevant amplitude/frequency parameter combinations:

Fig.5 shows two incidence variations for the two frequencies: f=2.5Hz and 5Hz respectively. A almost perfect sin-wave could only been achieved for the lower frequency whereas in the higher frequency case a saw-tooth type of incidence variation occurred. The latter is repeating accurately for all measured periods.

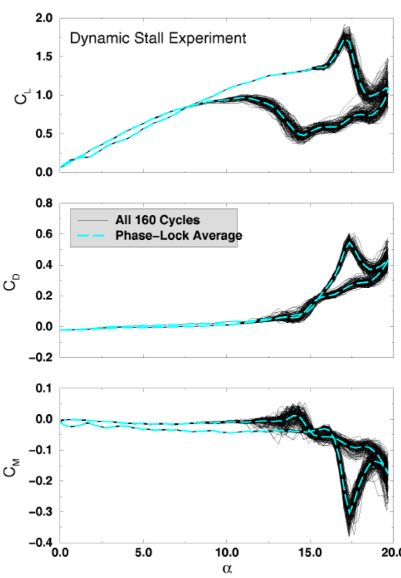

Fig.6: Total Measured Periods, Phase-Lock Average

The reduced frequency belonging to the saw-tooth variation (ω^*=0.1) is the more relevant one for helicopter applications. On the other hand it is not a difficult task to reproduce the saw-tooth incidence variation in the numerical code. The physical features of dynamic stall are very similar in the one or the other case. Therefore it was decided in the present discussion to concentrate on the saw-tooth incidence variation and use the higher reduced frequency correspondingly.

Fig.6 shows typical lift-,drag-and pitching moment hysteresis loops for M=0.31, ω^*=0.1 and $\alpha_0=10^o$,$\alpha_1=10^o$.

All 160 measured periods have been simply plotted on top of each other. In addition the phase-lock average of all loops has also been indicated in these plots. In the lower incidence regimes up to about 16^o all curves are included in a narrow line. With the start of dynamic stall and the development of a strong dynamic stall vortex, a steep increase of the lift beyond 16^o can be observed. In this region the curves are spreading and cover a quite large area, an effect which is increased in the following separated flow region. During the upper part of the down-stroke and down to about 10^o incidence the curve-spreading is established as well until in the low incidence part of down-stroke the curves merge again into one line. Fig.6 demonstrates the strong fluctuations in the air loads that correspond to flow separation. This information regarding the fluctuations is of course lost in the phase lock average data.

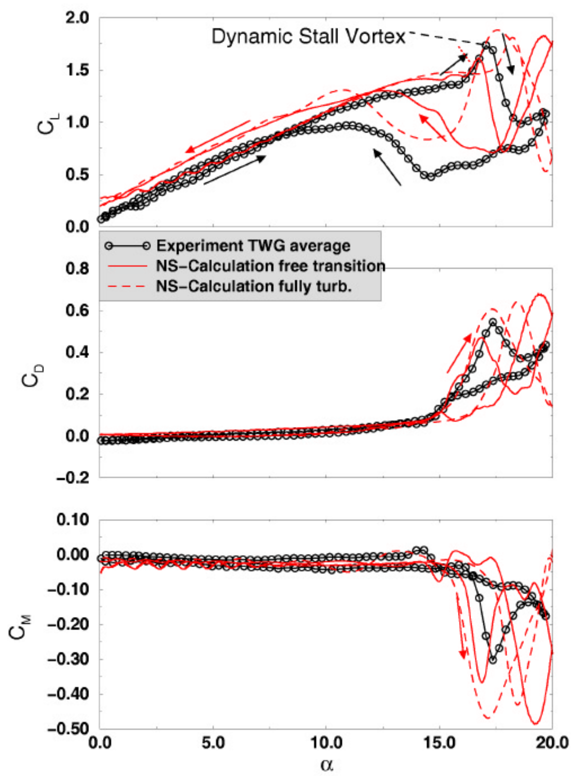

Fig.7: Lift-Drag- and Pitching Moment Hysteresis Loops, M=0.31, Re=1.15x10^6, ω^*=0.1.

$$\alpha=10^o+10^o \sin(\omega^*T)$$

However, the following discussions use only the average for comparison with the numerical data.

6.2.1 Mach=0.31

Mach 0.31 represents the lowest Mach number to be realized in the TWG wind tunnel. For this Mach number it is assumed that compressibility effects are not severe. **Fig.7** displays lift-drag- and pitching moment hystersesis loops from Fig.6 compared with numerical results achieved for 1) fully turbulent flow and 2) for free transition modelling. In this case wind tunnel wall adaptation has been applied for the $\alpha_0=10^o$ mean incidence.

The upstroke region shows very good correspondence with the experimental data. Deviations occur close to the formation of the dynamic stall vortex indicated by an extra peak in the lift curve (Fig.7,upper). Larger deviations occur in the separated region after the dynamic stall vortex has been shedded into the wake. A secondary peak in the forces and moment loops can be detected in this incidence regime. For the calculations strong differences occur between the fully turbulent assumption and the calculation with free transition. Modelling the free transition the correspondence to the experimental data is improved although the secondary peak is also existing in this case. The indication of a secondary peak can also be found in Fig. 6 where all curves are plotted. However the calculation shows the effect much more pronounced. The reason may be that the flow in unsteady and separated mode will always arrange in a 3D-manner. The 2D-flow assumption in the code would then no longer be valid. It is of importance to notice that during upstroke and formation of the dynamic stall vortex the two dimensionality of the flow seems to be a good approximation.

Simple transition modelling improves the results.

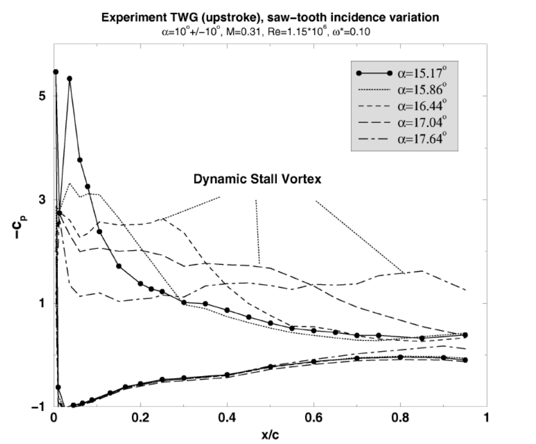

Fig.8: Measured Chord wise Pressure Distributions, Effect of Dynamic Stall Vortex

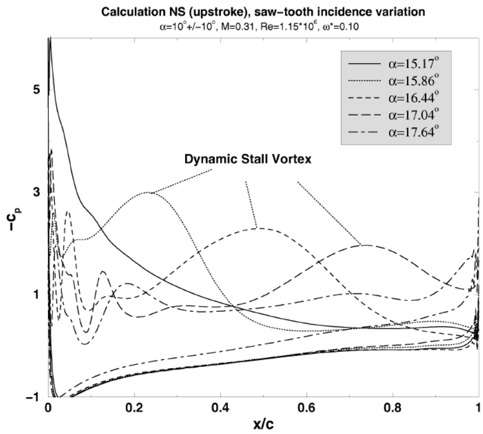

Fig 9: Calculated Chord wise Pressure Distribution, Effect of Dynamic Stall Vortex M=0.31

To investigate the upstroke region including the formation and shedding of the dynamic stall vortex more in detail some chord wise pressure distributions have been selected and plotted in **Fig.8** for the experiment and in **Fig.9** for the calculation.
In both figures the pressure distributions at the same incidences have been displayed for comparison. At α=15.17° the flow is attached in both experiment and calculation (note that in Fig.8 one pressure sensor shows a wrong signal at the leading edge). Close to 16° dynamic stall onset occurs with a sudden reduction of the leading edge pressure peak and the formation of an extra pressure peak which is moving over the airfoil upper surface with increasing incidence indicating the effect and movement of the dynamic stall vortex. Both calculation and experiment show very similar results with a slight phase lead of the numerical data (see also Fig.7).

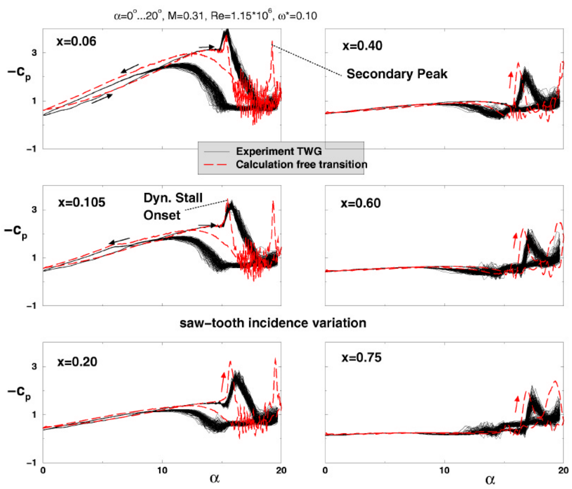

Fig.10: Calculated and Measured Pressure Hysteresis Loops at Selected x/c-Positions, M=0.31

The hysteresis loops of the static pressure at several positions on the airfoil upper surface have been plotted in **Fig.10** starting at x/c=0.05 to x/c=0.75. The extra peak due to the dynamic stall vortex can be found more clearly in the pressure loops. This peak almost matches the calculation (free transition). The simulation shows a secondary peak close to the maximum incidence which is also indicated in the experimental data but much less pronounced. In the down stroke regime both calculations and experiment show some wiggles which are dieing out towards the down stroke motion. The lower part of the down stroke is again represented by single lines. It should be pointed out here that the strong numerical wiggles are still representative because they are exactly repeating for additional periods of calculation.

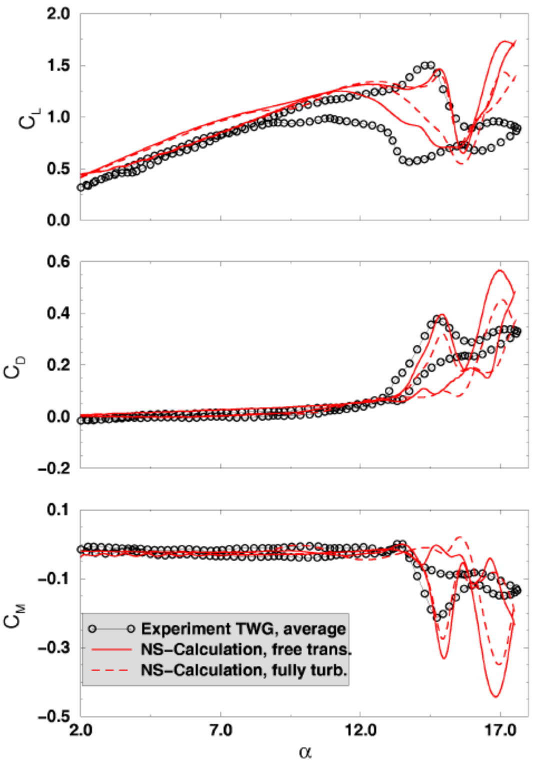

Fig.11: Lift-Drag- and Pitching Moment Hysteresis Loops, M=0.40, Re=1.44x10^6, α=10°+8° sin(ω*T)

6.2.2 Mach=0.40

Fig.11 shows force- and moment hystersis loops for the higher Mach number M=0.40. The plots include the same curves as Fig. 7 for the smaller Mach number. Now it is very obvious that the differences in calculations between the cases fully turbulent and free transition are much smaller than in the lower Mach number case (Fig.7). The reason for these effects will be discussed later. Again a good correspondence between calculation and measurement is found in the up stroke region up to dynamic stall onset and including the peak in lift, drag and moment. The secondary peak close to the maximum incidence is predicted again. The reattachment process during down stroke is

matching the experimental data even better than for the lower Mach number.
Fig. 12 (experiment) and **13** (calculation) show again the development of the instantaneous static pressure distributions at selected angles of attack during the development and movement of the dynamic stall vortex. Different to the lower Mach number (Figs. 8 and 9) the experimental data now phase-lead the calculation by about 0.5°. This can also be observed in the force and moment loops of Fig.11.

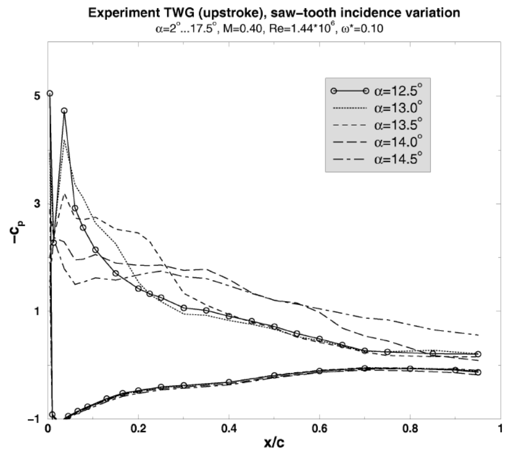

Fig.12: Measured Chord wise Pressure Distributions, Effect of Dynamic Stall Vortex M=0.31

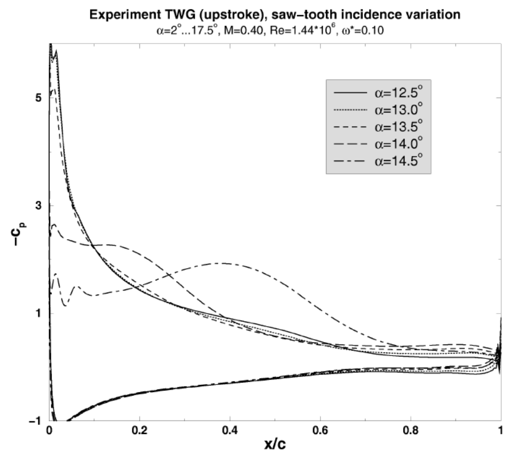

Fig.13: Calculated Chord wise Pressure Distributions, Effect of Dynamic Stall Vortex M=0.40

Fig.14 shows again pressure loops for some selected chord wise positions on the airfoil upper surface. Again a secondary pressure peak is developing which is only slightly indicated in the experimental data. The phase lead of dynamic stall onset for the experimental curves compared with the simulated ones can be observed also in the pressure loops.
Fig.15 displays calculated Mach contours for a certain incidence during upstroke. The white spots at the airfoil leading edge indicate supersonic flow in this region. One can see that for M=0.31 the supersonic bubble is quite small although existent. For the slightly higher Mach number a rather large supersonic area has developed which is terminated by a small but strong shock wave or system of shock waves. A similar behaviour was also observed in the experiments of [17].
These rather localized differences due to different inflow parameters develop in time and have a strong impact on the start of dynamic stall onset. In

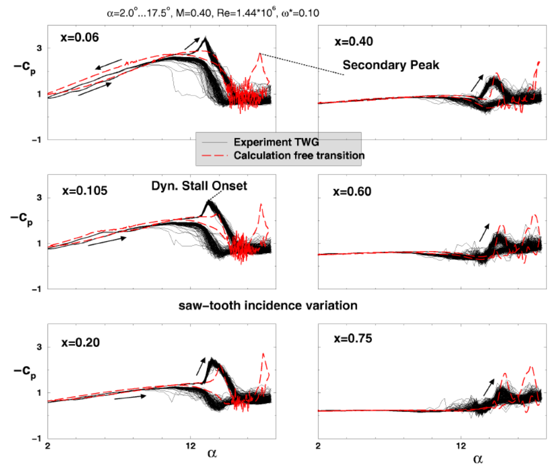

Fig.14: Calculated and Measured Pressure Hysteresis Loops at Selected x/c-Positions, M=0.40

the lower Mach number case dynamic stall onset is influenced mainly by the effects of transition. For the higher Mach number however shock induced separation occurs and triggers the dynamic stall onset. This can indirectly be observed in Fig.11 where calculations with and without transition lead to very similar results. The influence of transition in the lower Mach number case (see Fig.7) compared to fully turbulent calculations however is quite severe.

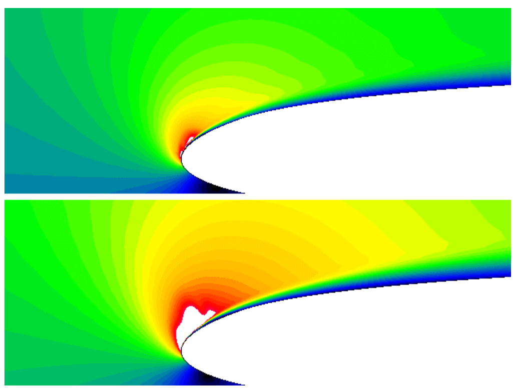

Fig.15: Mach contours, upper: M=0.31, α=14° Lower: M=0.40, α=13°

6.3 Wind Tunnel Wall Interference

As has been mentioned before, the experiments have been carried out in the adaptive-wall test section of the DNW-TWG wind tunnel. Wall adaptation is successfully applied for steady tests. However, in the case of an oscillating model when both the mean incidence and the amplitude are rather large, a simple and meaningful adaptation procedure is not available. Recent wind tunnel tests have shown that wall effects may have a large impact on forces and moment for dynamic stall measurements. It is therefore of interest to apply a procedure for dynamic stall tests which can easily be applied in the present adaptive wall applications.

It seems to be straightforward to use the mean incidence of oscillation as the incidence where steady adaptation is accomplished and then do the dynamic stall measurements with frozen wall shapes. However this procedure may fail if one does not take into account the specific flow physics occurring at dynamic stall.

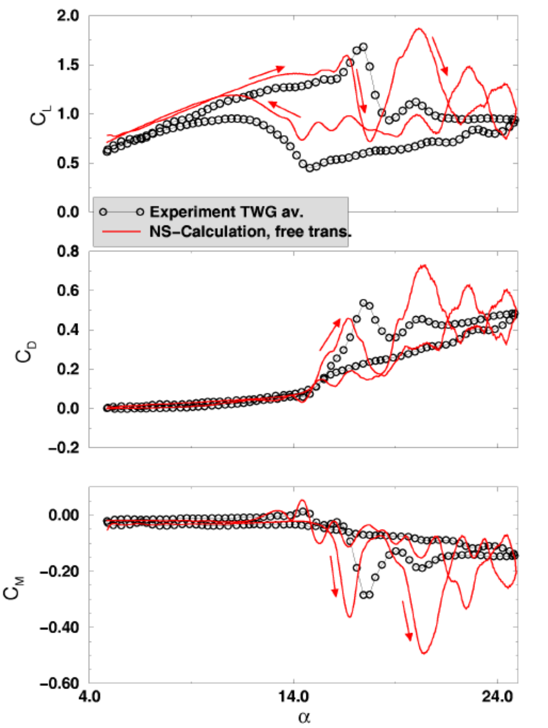

Fig.16: Lift-Drag- and Pitching Moment Hysteresis Loops, M=0.31, Re=1.15x10^6, α=15°+10°sin(ω*T), ω*=0.1

Fig.16 shows again lift-, drag and moment hysteresis loops for M=0.31 but with the incidence variation: α=15+/-10°, ω*=0.1, saw-tooth variation. Wall adaptation has been applied at the mean incidence, i.e. at α =15°. This incidence is located at the end of the linear lift versus incidence region. However the steady polar of Fig.3 clearly shows that at 15° the maximum lift for the present airfoil is already by far extended. Doing adaptation for 15° means that the flow is already strongly separated. Using this adaptation for the dynamic stall measurement as displayed in Fig.16 leads to a shift of the experimental data downwards to lower lift values. It must be kept in mind that due to the pitching motion of the airfoil separation is shifted considerably to higher incidences. But adaptation can only be applied for steady non-separated flow.

During the tests the sensors installed along the upper and lower adaptive walls have measured instantaneous pressure data. **Fig.17** shows for a selection of incidences during the up stroke as well as the down stroke motion the corresponding wall pressures for both upper and lower walls. The broad band shows the pressure distributions for steady wind tunnel wall adaption.

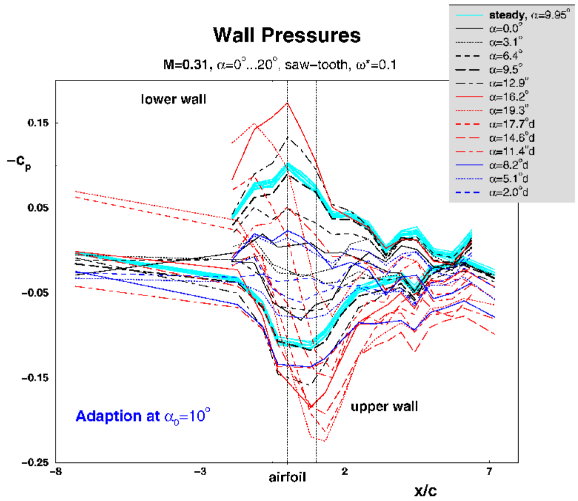

Fig.17a: Wind Tunnel Wall Pressure Distributions During Up-stroke Motion of Airfoil, M=0.31, Steady Adaptation at α=10°

In **Fig.17a** the adaptation has been performed at α=10° corresponding to Fig.7. Note that for this subsonic case the instantaneous pressure data at the same incidence as the wall adaptation was performed match to the pressure distribution at steady conditions.

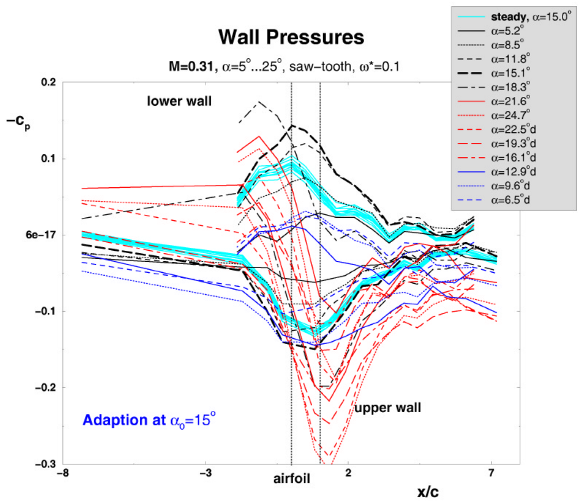

Fig.17b: Wind Tunnel Wall Pressure Distributions During Up-stroke Motion of Airfoil, M=0.31, Steady Adaptation at α=15°

The situation is somewhat different for the higher mean incidence of $\alpha=15^o$ as represented in **Fig.17b.** Now larger differences occur between the steady pressure data at 15^o and the instantaneous pressure distribution at the same incidence. In the steady case the flow is separated at 15^o, in the unsteady case the separation has not been started, the flow topology is therefore completely different.
If some fundamental rules are taken into account a wind-tunnel wall adaptation for a moving model under dynamic stall condition may have considerable benefits. The question whether the information of unsteady pressure data at the wall measured simultaneously with the unsteady pressure distribution of the oscillating model may lead to improved wall interference reductions can not be answered at the present time. It is possible that the wall and the model surface pressure data may serve as inputs for a kind of transfer function to determine local improvements of an instantaneous wall interference correction. Further effort is necessary to investigate this subject.

7. Conclusion

Comprehensive measurements on a model with a supercritical airfoil shape have been done in the adaptive-wall test section of the DNW-TWG transonic wind-tunnel facility at DLR-Göttingen. No stall, light stall and deep stall conditions have been investigated. Corresponding numerical calculations have been carried out and their results have been compared with the experimental data. It has been shown that boundary-layer turbulence and also laminar-turbulent transition modelling may have a considerable effect on the simulated data. A simple quasi-steady transition model has shown improvements compared to calculations with fully turbulent flow assumption.
Wind-tunnel wall adaptation in the test section of the wind tunnel has also been studied regarding its impact on dynamic-stall experiments. Some simple rules in application of wall adaptation in dynamic stall flow cases have been found. Improvements of wall correction methods for unsteady cases taking into account unsteady wall pressure data may have the potential for further improvements.
The present wind tunnel tests have also been a preparation test for the project ADASYS, a joint project between DLR, ECD and EADS. The main objective of the ADASYS project is to control dynamic stall by means of a moving and sealed leading edge flap. The experiences collected during the present test phase and during the data reduction and physical interpretation phase are of considerable benefit with respect to the complicated test phase within the project ADASYS.

8. References

[1] Sobieczky,H., "Geometrie Generator for Aerodynamic Design", CISM Course and Lectures No.366, 'New Design Concepts for High Speed Air Transport', Springer, Wien, New York (1997), pp.137-158.
[2] Schimke,D., Jänker,P., Wendt,V., Junker,B., "Wind tunnel evaluation of a full scale piezo-electric flap control unit", 24th European Rotorcraft Forum, Marseille, France, 15-17.September, 1998.
[3]Lorkowski,T., Jänker,P., Hermle,F., Storm,M., Christmann,M., Wettemann,M., "Development of a piezo-electrically actuated leading-edge flap for dynamic stall delay", 25th European Rotorcraft Forum, September, 14-16, 1999, Rome, Italy.
[4] Geissler,W., Sobieczky,H., Trenker,M., "New Rotor Airfoil Design Procedure for Unsteady Flow Control", 26th European Rotorcraft Forum, September,26-29,2000, The Hague, The Netherlands.
[5] Martin,P. ,Chandrasekhara,M.S., Geissler,W., "Dynamic stall measurements and computations for a VR-12 airfoil with a variable droop leading edge", paper 59th AHS Forum, May 6-8,2003, Phoenix, AZ.
[6] Geissler,W., Trenker,M., Sobieczky,H., "Active Dynamic Flow Control Studies on Rotor Blades", Research and Technology Agency, Spring 2000 Symposium on Active Control Technology, Braunschweig, Germany, 8-12.May, 2000.
[7] Geissler,W., "Instationäres Navier-Stokes Verfahren für beschleunigt bewegte Profile mit Ablösung (Unsteady Navier-Stokes Code for Accelerated Moving Airfoils with Separation) in German, DLR-FB 92-03, (1992).
[8] Wedemeyer,E., Taylor,N.J., Holst,H., "Adaptive wall techniques", AGARD AG 336, 1998.
[9] Cebeci,T., Bradshaw,P., "Momentum Transfer in Boundary Layers", McGraw-Hill, New York, 1979.
[10] Jacobs,M., "Treatment of the wall boundary layer in the wall adaptation procedure and steady wall adaptation for dynamic tests", Private communication, DNW BU GuK, Göttingen, 2002
[11] Schewe,G., "Force measurements in aeroelasticity using piezoelectric multicomponent transducers", Proc. IFASD, DGLR 91-06, Aachen, Germany, 1991.
[12] Beam,R., Warming,R.F., "An Implicit Factored Scheme for the Compressible Navier-Stokes Equations", AIAA J., Vol.16, No.4, Apr. 1978.
[13] Jameson,A.,Schmidt,W.,Turkel,E.,"Numerical Solution of the Euler Equations by Finite Volume Methods Using Runge Kutta Time-Stepping Schemes", AIAA Paper 81-1259, 1981.
[14] Spalart,P.R., Allmaras,S.R., "A One-Equation Turbulence Model for Aerodynamic Flows", AIAA-Paper 92-0439, 1992.
[15] Geissler,W., Ruiz-Calavera, L. P., "Transition and Turbulence Modelling of Dynamic Stall and Buffet", 4th International Symposium on Engineeing Turbulence Modelling and Measurements, Frantour&CCAS, Porticcio-Ajaccio, Corsica, France, 1999.

[16] Menter,F.R., “Improved two-equation k-omega Turbulence Models for Aerodynamic Flows”, NASA TM-103975, Oct. 1992.
[17] Wilder,M.C., Chandrasekhara,M.S., Carr,L.W., “Transition Effects on Compressible Dynamic Stall of Transiently Pitching Airfoils”, AIAA 24th Fluid Dynamic Conference, July 6-9,1993, Orlando ,FL.
[18] Geissler, W., Chandrasekhara, M. S., Platzer,M.F., Carr,L.W., “The Effect of Transition Modelling on the Prediction of Compressible Deep Dynamic Stall”, The Seventh Asian Congress of Fluid Mechanics, Dec.8-12, 1997, Chennai (Madras), India.